Author/s:
Saha, S;Rana, R;Nesterets, Y;Tahtali, M;de Hoog, F;Gureyev, T

Title:
Evaluating the performance of BSBL methodology for EEG source localization on a realistic head model

Date:
2017-03-01

Citation:
Saha, S., Rana, R., Nesterets, Y., Tahtali, M., de Hoog, F. & Gureyev, T. (2017). Evaluating the performance of BSBL methodology for EEG source localization on a realistic head model. International Journal of Imaging Systems and Technology, 27 (1), pp.46-56. https://doi.org/10.1002/ima.22209.

Persistent Link:
https://hdl.handle.net/11343/292571

Evaluating the Performance of BSBL Methodology for EEG Source Localization On a Realistic Head Model

Sajib Saha[1,2], Rajib Rana[4], Yakov Nesterets[2,3], Murat Tahtali[1], Frank de Hoog[5] and Timur Gureyev[6]

1) University of New South Wales, Canberra, Australia

2) CSIRO Manufacturing, Melbourne, Australia

3) University of New England, Armidale, Australia

4) Autonomous Systems Laboratory, CSIRO ICT Centre, Australia

5) CSIRO Data61, Canberra, ACT, Australia

6) ARC Centre of Excellence for Advanced Molecular Imaging, School of Physics, The University of Melbourne, Parkville, VIC 3010, Australia

S.Saha@student.adfa.edu.au, Rajib.Rana@usq.edu.au, Yakov.Nesterets@csiro.au, M.Tahtali@adfa.edu.au, Frank.Dehoog@csiro.au, Tim.Gureyev@csiro.au

Abstract In this paper we evaluate the performance of block sparse Bayesian learning (BSBL) ~~(Zhang *et al* 2012)~~ method for EEG source localization. By exploiting the internal block structure, the BSBL method solves the ill-posed inverse problem more efficiently than other methods that do not consider block structure. Simulation~~Numerical~~ experiments were conducted on a realistic head model obtained by segmentation of MRI images of the head. Two definitions of blocks were considered: Brodmann areas and automated anatomical labelling (AAL). The experiments were performed both with and without the presence of noise. Six different noise levels were considered having SNR values from 5 dB to 30 dB with 5dB increment. The evaluation reveals several~~few~~ potential findings – firstly, BSBL is more likely to produce better source localization than sparse Bayesian learning (SBL), however, this is true up until a limited ~~the maximum~~ number of simultaneously active areas only ~~must be less than a certain number~~. Experimental results show that for 71- channel electrodes setup BSBL outperforms SBL for up to three simultaneously active blocks. From four simultaneously active blocks SBL turns out to be marginally better and the difference between them is statistically insignificant. Secondly, different anatomical block structures such as Brodmann areas or AAL does not seem to produce any

significant difference in EEG source localization relying on BSBL. Thirdly, even when the block partitions are not known exactly BSBL ensures better localization than SBL as soon as block structure persists in the signal.

Keywords Electroencephalography, source localization, Brodmann map, automated anatomical labelling, sparse reconstruction, BSBL

1. Introduction

The problem of source localization in electroencephalography (EEG) has gained significant attention in recent years because of its potential diagnostic value for epilepsy (Plummer *et al* 2008), stroke (Finnigan *et al* 2013, Phan *et al* 2012), traumatic brain injury (Kaplan *et al* 2011) and other brain disorders. Localization of the sources of electrical activity inside the brain works by measuring the scalp potentials produced by the electric activity in the brain, and then estimating the dipoles that best fit the measurements. ~~Mathematical~~ Dipoles are used to approximate the coherent electrical activities of certain neuronal population within a small volume of the brain and in principle consideration of more dipoles should give more accurate results. However consideration of large number of dipoles significantly increases the dimensionality of the problem. The EEG source localization represents a high-dimensional inverse problem, which is severely ill-posed (Nunez *et al* 1994, Nunez *et al* 2006, Jatoi *et al* 2014) and has an infinite number of solutions (Wu *et al* 2013). In order to find an appropriate unique solution, among the set of possible ones, constraints are applied into the problem (Grech *et al* 2008). In the literature, the most commonly used constraint is the minimum-norm constraint (Pascual-Marqui *et al* 1999, Phillips *et al* 1997, Gençer *et al* 1998), which finds the solution that best matches the measurements with the smallest l_2 norm residuals. The strength of l_2 norm based approaches is their low computational cost; however such methods are often criticized for generating very broadly distributed or "smeared" sources in the reconstruction region (Gramfort *et al* 2012) and for poor performance for multiple simultaneously active sources (Wagner *et al* 2004, Saha *et al* 2015). As an alternative to l_2 norm based approaches, l_1 norm based approaches are also used nowadays. While l_1 norm based approaches can produce focal sources, they are very computationally intensive. Importantly both l_1 and l_2 norm based approaches have their own specific applications (Liu *et al* 2015).

Relying on the drastic development of computational power, in the last two decades, significant efforts have been made to solve ill-posed problems based on l_1 norm constraint. Techniques relying on l_1 norm constraint return a solution vector that not only matches the measurements, but is also sparse (has as few nonzero entries as

possible) . Focal underdetermined system solver (FOCUSS) is a classic example of this category, which uses a weighted minimum norm (MN) approach for sequentially reinforcing strong sources and suppressing the weak ones (Gorodnitsky *et al* 1995). Other interesting algorithms are based on iterative reweighted least-squares (IRLS) methods, which are similar to FOCUSS and are based on iteratively computing weighted MN solutions with weights updated after each iteration (Li *et al* 1993, Daubechies *et al* 2008). The homotopy method by Osborne (Osborne *et al* 2000) and LARS-LASSO algorithm (Tibshirani 1996, Efron *et al* 2004) (a variant of the homotopy method) are extremely powerful methods for solving the l_1 norm problem. Simple coordinate descent methods (Friedman *et al* 2004) or block wise coordinate descent, also called block coordinate relaxation (Bruce *et al* 1998), alternating direction method of multipliers (ADMM) by Boyd *et al* (Boyd *et al* 2011), and forward-backward splitting method by Goldstein *et al* (Goldstein *et al* 2014) are also very successful strategies. When the problem is highly ill-posed and the signal has a structure, a trend in the field of sparse signal recovery is to exploit the structure of the signal for better performance (Zhang *et al* 2012). Block sparse signal recovery relies on the same mathematical paradigm of sparse signal recovery; however considers the signal as a collection of few nonzero blocks, where a block is a collection of consecutive nonzero entries. A number of algorithms exists in the literature that rely on block structure, and exploit the correlation within the block for better performance - such as mixed l_2/l_1 program (Eldar *et al* 2009), block-OMP (Eldar *et al* 2010), block-CoSaMp (Baraniuk *et al* 2010) and block sparse Bayesian learning (BSBL) (Zhang *et al* 2012).

An interesting study about the performance of several state of the art sparse recovery algorithms for solving EEG source localization problem has been done by, Zhang in (Zhang *et al.* 2012). In EEG, researchers have used sparse prior as constraints in spatial, spatiotemporal and frequency domains to reflect the focal nature of the cortical activity (Saha *et al* 2015b). Ding *et al* in (Ding *et al* 2009, 2013) have proposed an l_1-norm electromagnetic source imaging method by exploring sparseness in a transform domain. To efficiently incorporate the sparsity prior Chang *et al* in (Chang *et al* 2010) have considered Laplacian and Spherical wavelet transform to solve the localization problem in MEG (magnetoencephalography). Wu *et al* in (Wu *et al* 2013) have proposed a matching pursuit based solution to the EEG inverse problem. While it produces better localization compared to the state-of-the art methods, the number of sources needs to be known a priori for the refinement of the localization in this method. Despite the growing interest, the applicability of sparsity-enforcing priors for EEG source localization is still limited because of the significantly smaller number of electrodes compared to the typical number of virtual electric current dipoles under consideration.

Bayesian algorithms (Friston *et al* 2008, Lopez *et al* 2012, Lopez *et al* 2014) are also found successful in the context of EEG source localization. In (Zhang 2012), Zhang has shown that in EEG, where the lead field matrix is highly coherent (Saha *et al* 2105b), sparse Bayesian learning (SBL) seems to outperform other state-of-the-art sparsity prior approaches. ~~Since EEG source localization is severely ill-posed, in this paper we focus on block sparse recovery using BSBL.~~When block structure is very likely within the signal, an even better strategy is block sparse Bayesian learning (Zhang *et al* 2012). It is well accepted in the literature that cerebral sources of scalp EEG spikes are resultant from activation of sources that fall within a broad region of the brain (Nunez *et al* 2006). In (Tao *et al* 2005), Tao *et al* have shown that in 90% cases scalp EEG spikes are associated with a source area of greater than 10 cm^2. Thus it seems a logical choice to consider several dipoles as a block when many of them falls within the defined source area. In this paper we evaluate the performance of BSBL method over SBL method in the context of EEG source localization, where Brodmann area (Zilles *et al* 2010) and automated anatomical labelling (AAL) (Tzourio-Mazoyer *et al* 2002) are used to define blocks.

Specific contribution of the paper includes:

i) Systematic evaluation of SBL and BSBL methods in the context EEG source localization by varying the number of simultaneously active blocks, with and without noise in generated EEG signals.

ii) Use of a realistic head model that was obtained from the segmentation of MRI images of the head.

ii) Use of Brodmann areas and AAL to define blocks separately. It is worth mentioning, the AAL map is frequently used in functional Magnetic Resonance Imaging (fMRI) to describe out the region of interest (Desikan *et al* 2006, Saha *et al* 2015c), which indicates the potential suitability of such segmentation of the brain as a tentative basis to define blocks relevant to EEG. Brodmann areas were originally defined on the basis of the cytoarchitectural, rather than functional organization of the neurons in the cerebral cortex, however recent studies have unveiled the structural–functional correlations of many Brodmann areas, and thus point to the potential suitability of such segmentation of the brain as a tentative basis for a functional classification relevant to EEG (Zilles *et al* 2010, Saha *et al* 2014). ~~Assuming that block structure is highly likely in EEG, this study aims to analyze the performance improvement of BSBL method over SBL method. The experiments were performed on a realistic head model obtained from the segmentation of MRI images of the head. Brodmann areas (BA) (Brodmann *et al* 1909) and automated anatomical labelling (AAL) (Tzourio-Mazoyer *et al* 2002) were used separately to define blocks. Experiments were performed by varying the number of simultaneously active blocks, with and without noise in generated EEG signals.~~

1.1. Head Modelling

EEG source localization requires a proper modeling of the head to be carried out by using analytical method or by using numerical method. Analytical method uses spherical head modelling with homogeneous conductivity for each sphere. Numerical methods are provided with much more realistic modelling of the head. Due to complicated geometries and conductivity distribution, the computational complexity of the numerical methods is high, however yields more accurate solutions with high resolution and low localization error. Commonly used numerical methods are finite element method (FEM) (Jatoi *et al* 2013), boundary element method (BEM) (Jatoi *et al* 2015) and finite difference method (FDM) (Jatoi *et al* 2016). With tfehe FDM volume conduction model, the mapping between MRI image and FDM voxels is pretty straight forward (Jatoi *et al* 2016), and is used in this paper.

2. Material and Methods

2.1. Recovery of Block Sparse Signal Using BSBL

The mathematical formulation of the EEG inverse problem has the following form (Pascual-Marqui 2002, Pascual-Marqui 1999):

$$\boldsymbol{\Phi} = \boldsymbol{KJ} + \boldsymbol{n}, \tag{1}$$

where $\boldsymbol{\Phi} \in \mathbb{R}^{N_E \times 1}$ is the measurement ~~vector~~ potentials consisting of N_E measurements equal to the number of electrodes, $\boldsymbol{K} \in \mathbb{R}^{N_E \times M}$ is the known lead field matrix ($N_E << M$), M is the number of unknowns, $\boldsymbol{J}$ is the primary or impressed current density vector and $\boldsymbol{n}$ is the noise vector. BSBL assumes the signal $\boldsymbol{J}$ has the following block structure:

$$\boldsymbol{J} = [\underbrace{J_1, \dots, J_{d_1}}_{\boldsymbol{J}^{1^T}}, \dots, \underbrace{J_{d_{g-1}+1}, \dots, J_{d_g}}_{\boldsymbol{J}^{g^T}}]^T. \tag{2}$$

The block partition in (2), $d_1, \dots, d_g$ are not necessarily identical and among the g blocks only a few blocks are nonzero. Relying on the internal block structure of the signal, two efficient recovery algorithms are proposed in (Zhang *et al* 2012). Out of the two algorithms proposed in (Zhang *et al* 2012) we focus on the algorithm that

was directly derived from the bSBL framework (Zhang *et al* 2011) and requires a priori knowledge of the block partition and performs better than the other.

BSBL (Zhang *et al* 2012) describess each block $\boldsymbol{J}^i \in \mathbb{R}^{d_i \times 1}$ using a parameterized multivariate Gaussian distribution:

$$p(\boldsymbol{J}^i) \sim \mathcal{N}(0, \gamma_i \boldsymbol{B}_i); i = 1, \dots, g,$$

where γ_i is a non-negative parameter, and $\boldsymbol{B}_i \in \mathbb{R}^{d_i \times d_i}$ is a positive definite matrix, capturing the correlation structure of the *i*-th block. When $\gamma_i = 0$, the *i*-th block becomes zero. During the learning process most γ_i tend to be zero, due to the mechanism of automatic relevance determination (Tipping 2001, Zhang *et al* 2013). Thus sparsity at the block level is ensured (Zhang *et al* 2013). Moreover by assuming that different blocks are mutually uncorrelated, the prior for $\boldsymbol{J}$ is given by $p(\boldsymbol{J}) \sim \mathcal{N}(\boldsymbol{0}, \boldsymbol{\Psi}_0)$, where $\boldsymbol{\Psi}_0$ is a block diagonal matrix with each principal block given by $\gamma_i B_i$. The measurement noise vector is assumed to satisfy $p(\boldsymbol{n}) \sim \mathcal{N}(\boldsymbol{0}, \lambda \boldsymbol{I})$, where λ is a non-negative scalar and $\boldsymbol{I}$ is the identity matrix. The posterior of $\boldsymbol{J}$ is given by $p(\boldsymbol{J}|\boldsymbol{\Phi}) = \mathcal{N}(\boldsymbol{\mu}_J, \boldsymbol{\Psi}_J)$ with $\boldsymbol{\mu}_J = \boldsymbol{\Psi}_0 \boldsymbol{K}^T (\lambda \boldsymbol{I} + \boldsymbol{K} \boldsymbol{\Psi}_0 \boldsymbol{K}^T)^{-1} \boldsymbol{\Phi}$ and $\boldsymbol{\Psi}_J = (\boldsymbol{\Psi}_0{}^{-1} + \frac{1}{\lambda} \boldsymbol{K}^T \boldsymbol{K})^{-1}$. Once the parameters $\lambda, \gamma_i, \boldsymbol{B}_i$ (for $i = 1, \dots, g$) are estimated the maximum-a-posterior (MAP) estimate of $\boldsymbol{J}$ can be directly obtained from the mean of the posterior. Expectation maximization (EM) method is applied to learn the parameters (Zhang *et al* 2011). Finally, following Zhang *et al* (Zhang *et al* 2012), the iterative algorithm of the BSBL methodology can be described as follows:

$$\boldsymbol{\mu}_J \leftarrow \boldsymbol{\Psi}_0 \boldsymbol{K}^T (\lambda \boldsymbol{I} + \boldsymbol{K} \boldsymbol{\Psi}_0 \boldsymbol{K}^T)^{-1} \boldsymbol{\Phi}$$

$$\boldsymbol{\Psi}_J \leftarrow \boldsymbol{\Psi}_0 - \boldsymbol{\Psi}_0 \boldsymbol{K}^T (\lambda \boldsymbol{I} + \boldsymbol{K} \boldsymbol{\Psi}_0 \boldsymbol{K}^T)^{-1} \boldsymbol{K} \boldsymbol{\Psi}_0$$

$$\lambda \leftarrow \frac{||\boldsymbol{\Phi} - \boldsymbol{K}\boldsymbol{\mu}_J||_2^2 + \lambda[M - \mathrm{Tr}(\boldsymbol{\Psi}_J \boldsymbol{\Psi}_0{}^{-1})]}{N_E}$$

$$\gamma_i \leftarrow \frac{1}{d_i} \mathrm{Tr}\left[\boldsymbol{B}_i{}^{-1} \left(\boldsymbol{\Psi}_J{}^i + \boldsymbol{\mu}_J{}^i (\boldsymbol{\mu}_J{}^i)^T\right)\right];\ \forall_i \in 1{:}\, g$$

$$\boldsymbol{B}_i \leftarrow \frac{\boldsymbol{\Psi}_J{}^i + \boldsymbol{\mu}_J{}^i (\boldsymbol{\mu}_J{}^i)^T}{\gamma_i};\ \forall_i \in 1{:}\, g$$

where $\boldsymbol{\mu}_J{}^i$ corresponds to the *i*-th block in $\boldsymbol{\mu}_J$ and $\boldsymbol{\Psi}_J{}^i$ corresponds to the *i*-th principal diagonal block in $\boldsymbol{\Psi}_J$. Once the algorithm converges, the estimate of $\boldsymbol{J}$ is given by $\boldsymbol{\mu}_J$.

2.2. Data Model and Assumptions

~~Numerical~~ Simulation experiments were conducted using a realistic head model that was obtained by segmentation of MRI images of the head and included four different major components, namely scalp, skull, cerebrospinal fluid (CSF) and brain tissue with the following relative conductivity values (Nunez *et al* 2006): $\sigma_{scalp}=1$, $\sigma_{skull}=0.05$, $\sigma_{CSF}=5$, $\sigma_{brain}=1$. The lead-field matrix was calculated using the MUDPACK-2 package (Adams 1989, 1989b) that implements the finite difference (multigrid) approach for solving elliptic partial differential equations. When using MUDPACK, the numeric grid had 1.25 mm step and the grid volume was 320×320×320 mm3 (i.e. 257×257×257 grid points). The source space was constructed by dividing the head model into cubes with a size of 15×15×15 mm^3 cubes and considering possible current dipoles only in the center of those cubes that consisted of at least 60% of gray matter. This segmentation procedure resulted in 230 dipole positions as shown in Figure 1.

To be consistent with the BSBL framework these 230 dipoles were clustered into blocks based on Brodmann areas (Brodmann *et al* 1909) and automated anatomical labeling (Tzourio-Mazoyer *et al* 2002) separately. Brodmann's map of the human cortex contains 86 cytoarchitectonic areas in total (considering the left and right half as separate areas), however for the head model considered we were able to form only 67 clusters. This is due to the coarse sampling of the head model and the threshold percentage of gray matter used to introduce a dipole; this resulted in the absence of dipoles in small Brodmann areas. For the AAL based clustering we used the template of the MRIcro (MRIcroAAL) package. The template consists of 116 areas in the standard MNI space. However for the head model considered we were able to form only 97 clusters. The resultant reduction of the number of clusters is due to the coarse sampling of the head model in EEG compared to fMRI and also due to the percentage of gray matter associated with a dipole.

It is worth mentioning that on a realistic head model as is considered in this paper, it is more typical to consider 5×5×5 mm^3 grid which gives about 6000 dipoles (Phan *et al* 2012, Saha *et al* 2105). However the coarse sampling in this work has been biased by the number of unknowns (i.e. 512) that was used in (Zhang *et al* 2012) for the evaluation of BSBL method. The considered sampling in this work resulted in 690 (=3×230) unknowns and provided a well tradeoff between the number of unknowns and the maximum number of Brodmann areas and AAL clusters that could be formed.

2.3. Source Localization

In order to localize the sources of electrical activity or more specifically to localize the blocks that are active, we solved the inverse problem based on BSBL (Zhang *et al* 2012) methodology. The solution $\hat{\boldsymbol{J}} \in \mathbb{R}^{690\times 1}$ was a component vector representing current sources at 230 locations within the brain volume with three directional (i.e. x, y, z directions) components per location. The x, y and z components are used to calculate the magnitude, $d = \sqrt{x^2 + y^2 + z^2}$ of the current density for each of the 230 dipoles. The magnitude of each of the blocks is computed by taking the summation of the magnitudes of all the dipoles that belongs to the block. We thus formed a vector $\xi \in \mathbb{R}^{N_B\times 1}$ presenting the strength (i.e. magnitude) of the blocks. $N_B = 67$ for BA based clustering or 97 for AAL based clustering. To determine the blocks that were active we first computed the maximum strength of ξ and we called this maximum strength as $\xi_{\max}$. From ξ we determined the blocks that had magnitudes ~~From the magnitudes of the blocks $|\boldsymbol{J}_{\boldsymbol{Block}}| \in \mathbb{R}^{N_B\times 1}$, the maximum magnitude, $|\boldsymbol{J}_{\boldsymbol{Block}}|_{\max}$ is determined, any block with a magnitude~~ larger than or equal to $t \times \xi_{\max}$ ~~$|\boldsymbol{J}_{\boldsymbol{Block}}|_{\max}$.~~ and we considered them active. ~~is considered to be active. $N_B = 67$ for BA based clustering or 97 for AAL based clustering.~~ Here~~T~~ the relative threshold, ~~t~~, was experimentally set to 1/3. It is worth clarifying that t has no consequence on the quality of reconstruction, and the chosen value provideds a good choice to suppress the unwanted maxima (if there was any) by keeping the actual ones.

3. Experiments and Results

~~Numerical~~ Simulation experiments were conducted by varying the number of simultaneously active blocks for the 71-channel EEG headset configuration shown in Figure 3. For each of two block structures (i.e. Brodmann areas or AAL), we considered two different cases: Case-I where we considered all that all dipoles of the active block had the same orientation, and Case-II where we assumed that dipoles of the active block were randomly oriented. In both of cases, all dipoles of the active block had identical magnitudes irrespective of their orientations.

Experimental data are likely to be contaminated with "noise" from various sources, including measurement noise and background brain activity (Liu *et al* 2015). For this reason, we also investigated the effect of simulated pseudo-random measurement noise superimposed on the calculated scalp potentials.

The noise vector $\boldsymbol{n}$ was generated based on the SNR (signal-to-noise ratio) defined below:

$$\text{SNR (in dB)} = 20\log_{10}\frac{||\boldsymbol{KJ}||_2}{<||\boldsymbol{n}||_2>}, \quad (3)$$

where <…> designates the mean value over a statistical ensemble. In this study we generated SNR values from 5 dB to 30 dB with 5dB increment.

Error distance (ED) (Yao *et al* 2005) was used to analyse the localization performance. Given two vectors $\boldsymbol{P} \in \mathbb{R}^{N_B \times 1}$ and $\boldsymbol{Q} \in \mathbb{R}^{N_B \times 1}$, the error distance between them are defined as below:

$$\text{ED} = \frac{1}{N_I} \times \sum_{i \in I}^{N_I} \min_l \left||r_i - s_l|\right| + \frac{1}{N_L} \times \sum_{l \in L}^{N_L} \min_i \left||s_l - r_i|\right|. \quad (4)$$

Here $\boldsymbol{s}_l$ and $\boldsymbol{r}_i$ are the centroid of the actual and estimated active blocks respectively. N_I and N_L are the total numbers of estimated and the undetected sources (i.e. active blocks) respectively. The first term of equation (4) calculates the mean of the distance from each estimated source to its closest real source, and the corresponding real source is then marked as detected. All undetected real sources made up the elements of the data set *L* and thus the second term in eq (4) is the mean distance from each of the undetected sources to the closest estimated source.

3.1 Single Block Activation

In this case to generate the forward problem, a single block was made active (more specifically all the dipoles in the block were active) and the corresponding potentials on the electrodes were calculated. The experiment was conducted for all the blocks activated sequentially one at a time. For each experiment we claimed a 'success' if the activated block was exactly localized in the reconstructed signal. The success rate was computed as $\frac{\sum_{i=1}^{N_{Blocks}}(ED^i==0)}{N_{Blocks}}$. For the unsuccessful cases we computed the 'error distance' between the vectors representing the actual and estimated active blocks. Taking into account all unsuccessful cases, we computed the mean error distance as $\frac{\sum_{i=1}^{N_{Blocks}}(ED^i)}{N_{unsuccessful}}$ and the standard deviation of the mean error distance. While generating the forward problem the dipole orientations were generated randomly, and, the whole experiment was repeated 1000 times. Table 1 represents the average of 1000 such findings, for noise free electrode dada. Figure 4 shows the success rate and localization error in the presence of different levels of noise.

From the results it is observed that when block structure persists in the signal, BSBL (Zhang *et al* 2012) outperforms SBL (i.e. BSBL with $\boldsymbol{B}_i \in \mathbb{R}^{1\times1}$). When a single block of dipoles is active, it is very likely to be exactly localized by the BSBL method. We also observe that when all the dipoles of the active block follows the same orientation (i.e. case-I) the chances of exact localization are higher in comparison to when all the dipoles of the active block follows the different orientation (i.e. case-II). Interestingly, the performance of exact localization is marginally better for AAL based blocks than for Brodmann area based blocks, although Brodmann area based blocks produces a system, which is comparatively less ill-posed. It appears that, grouping of dipoles based on Brodmann area produces a few blocks with significantly large number of dipoles in comparison to others (as can be seen from Figure 2) and when all the dipoles of such a large blocks is active, in addition with the actual active block a few surrounding blocks are detected as active in the reconstructed signal. These unwanted blocks result in the slightly decreased performance for Brodmann area based blocks in comparison to AAL based blocks. In the presence of noise significant decrease in localization accuracy is observable, which is equally applicable for all the cases in consideration. BSBL outperforms SBL.

3.2. Multi Block Activation

In this case S (S >1) blocks were activated simultaneously. From the total $C_S^{N_B} = \frac{N_B!}{S!(N_B-S)!}$ possible combinations of blocks, one combination was chosen randomly. We determined the block that had the minimum number of dipoles and considered only that many active dipoles for all the blocks. This was to make sure all the blocks that were made simultaneously active have same strength. We computed the error distance between the vectors representing the actual and estimated blocks and claimed a "success" if the computed error distance was zero. We did the experiment 1000 times (varying the combinations of activated blocks and the orientation of the average dipole moment) and the success rate was computed over these 1000 runs as $\frac{\sum_{i=1}^{1000}(ED^i==0)}{1000}$. For the unsuccessful cases we computed the mean error distance, $\overline{ED} = \frac{\sum_{i=1}^{1000} ED^i}{N_{unsuccessful}}$ and the standard deviation of the mean error distance. We followed this procedure for each value of S. Figure 5 shows the average of 1000 such findings without the presence of noise.

From the results it is observable that BSBL is likely to outperform SBL method when block structures actually persists in the EEG signal, however, this is only true for a limited number of simultaneously active blocks. For

the experiment here, up to two simultaneously active blocks the overall localization error (i.e. (1−Success Rate)×Localization Error) of BSBL (about 12 mm (i.e. average of the overall localization error produced by BSBL for the 4 different scenarios)) is significantly better than SBL (about 22 mm (i.e. average of the overall localization error produced by SBL for the 4 different scenarios)). For three simultaneously active blocks the performance of BSBL (overall localization error about 34 mm) is marginally better than SBL (overall localization error about 37 mm). From four simultaneously active blocks the performance of SBL is better than BSBL, however the difference is not to an extent that would be relevant in practice when considering the overall localization error which is already high enough for both of the methods. Figure 5 also reveals that better localization accuracy is more likely for case-I in comparison to case-II. Similar to the previous experiment, AAL based blocks performs better compared to Brodmann area based blocks. Figures 6 and 7 show a few representative reconstructions by different methods for case I.

Figure 8 represents the success rate and localization error (for unsuccessful cases) in the presence 20 dB noise.

While an overall decrease in localization accuracy is observable in Figure 8 in comparison to the Figure 5, noise does not seem to change the verdict that are already made in noiseless environment.

3.3. Exact Knowledge of Block Partition and Signal Reconstruction

In this part of the experiment we analyzed the performance of BSBL when block partition was not exactly known. Forward problems were generated as in section 3~~5~~.1 and 3~~5~~.2 however while solving the inverse problem rather than considering known Brodmann area or AAL based blocks, we considered arbitrary blocks of three consecutive dipoles. These arbitrary blocks were not aligned with the blocks that were used to generate the forward problem. The consideration of three consecutive dipoles to define a block had been biased by the average number of dipoles that could be distributed to the blocks. After solving the inverse problem using BSBL we computed the mean square error between $\boldsymbol{J}$ and $\hat{\boldsymbol{J}}$. For comparison the corresponding errors by using SBL and BSBL with exactly known partitions, were also computed. Figure 9 shows the findings for case I.

From the results it is observable that unsurprisingly when the partition of the blocks are known exactly BSBL out performs SBL at least for up to three simultaneously active blocks. When the block partitions are not known exactly, still BSBL performs better as long as block structure persist in the signal. No significant difference between Brodmann area and AAL based blocks are observed.

4. Discussions and Conclusion

~~Inspired by the findings by the authors in (Zhang *et al* 2012), i~~In this study we have quantitatively analyzed and evaluated the performance of BSBL method for EEG source localization using~~on~~ a realistic head model. We have considered two different block structures namely Bro~~a~~dmann areas and AAL~~, and have performed the experiments with and without the presence of noise~~. ~~Since the full functionality of different parts of the human brain is still not known completely~~, ~~blocks based on~~ Bro~~a~~dmann areas and AAL, which are cytoarchitectural and anatomical classification methods respectively, have got the significant potential to be considered as blocks. ~~, which is a cytoarchitectural classification method and an anatomical classification method, respectively, seems to be a reasonable choice. Nevertheless, numerous recent studies have unveiled the potential suitability of Broadmann segmentation of the brain as a tentative basis for a functional classification relevant to EEG (Zilles *et al* 2010). Similarly, AAL map (Tzourio-Mazoyer *et al* 2002) is frequently used in fMRI to describe the region of interest (Desikan *et al* 2008), which indicates its potential to become a tentative basis for functional classification relevant to EEG.~~ We evaluated the performance of the BSBL method by varying the number of simultaneously activated blocks and in regard to different levels of noise. Six different noise levels were considered having SNR values from 5 dB to 30 dB with 5dB increment.

The BSBL code implemented in MATLAB was downloaded from the author's website (http://dsp.ucsd.edu/~zhilin/BSBL.html). We have amended the code accordingly to work in conjunction with Brodmann area and AAL based blocks. For comparison, we also considered a variant of BSBL method, namely SBL without considering the blocks (i.e. $\boldsymbol{B}_i \in \mathbb{R}^{1\times 1}$).

The evaluation reveals several~~few~~ potential findings – firstly, BSBL is more likely to produce better source localization than sparse Bayesian learning (SBL), however the maximum number of simultaneously active areas must be less than a certain number. Experimental results show that for a single active block with uniform orientation of all the dipoles within the block, BSBL produces exact localization for around 95% cases in the absence of noise where as SBL produces exact localization for around 70% cases. In the presence of multiple simultaneously active blocks BSBL outperforms SBL up until three active blocks. From four simultaneously active blocks SBL turns out to be marginally better and the difference between them is statistically insignificant. In the presence of noise significant decrease of localization performance is observable which is equally applicable both for BSBL and SBL. However, BSBL still outperforms SBL. Secondly, different anatomical

block structures such as Brodmann areas or AAL does not seem to produce any significant difference in EEG source localization. While experiments 3~~5~~.1 and 3~~5~~.2 show the marginal better performance of AAL based blocks in comparison to Bro~~a~~dmann area based bocks, section 3~~5~~.3 shows it is not always trivial. Nevertheless in all the cases the difference between Bro~~a~~dmann area and AAL based blocks are not to an extent that would be relevant in practice. Thirdly, BSBL also outperforms SBL even when the block partitions are not exactly known as soon as the block structure persists in the signal.

From the experimental findings and from the considerations put forward in the experiment, we can conclude that in the context of EEG source localization BSBL solves the inverse problem more efficiently than SBL method. However, the improvement is limited and further improvement is a must before such method can be applied for multiple (>2) source localization.

Acknowledgment

This project was supported by the Computational and Simulation Sciences Transformational Capability Platform of Commonwealth Scientific and Industrial Research Organisation (CSIRO), Australia, along with University of New South Wales (UNSW), Canberra, Australia. The authors would like to thank Dr. Chao Suo and Dr. Roger Koenig-Robert of Monash Biomedical Imaging (MBI) Laboratory, VIC, Australia for their valuable comments and suggestions.

References:

J. C. Adams, MUDPACK: multigrid portable FORTRAN software for the efficient solution of linear elliptic partial differential equations, Applied Mathematics and Computation 34(2), 1989, pp. 113-146.

J. C. Adams, FMG results with the multigrid software package MUDPACK, 1989b.

R. Baraniuk, V. Cevher, M. Duarte, and C. Hegde, Model-based compressive sensing, IEEE Trans. on Information Theory, 56 (4), 2010, pp. 1982–2001.

S. Boyd, N. Parikh, E. Chu, B. Peleato, and J. Eckstein, Distributed optimization and statistical learning via the alternating direction method of multipliers, Foundations and Trends® in Machine Learning 3(1), 2011, pp. 1-122.

K. Brodmann, Vergleichende Lokalisationslehre der Großhirnrinde in ihren Prinzipien dargestellt auf Grund des Zellenbaues (Barth, Leipzig, 1909); English translation available in L. J. Garey, Brodmann's Localization in the Cerebral Cortex, Smith Gordon, London, 1994.

A. G. Bruce, S. Sardy, and P. Tseng, Block coordinate relaxation methods for nonparamatric signal denoising, Aerospace/Defense Sensing and Controls International Society for Optics and Photonics, 1998.

E. J. Candès, J. Romberg, and T. Tao, Robust uncertainty principles: Exact signal reconstruction from highly incomplete frequency information, IEEE Transactions on Information Theory, 52 (2), 2006, pp. 489-509.

W. Chang, A. Nummenmaa, J. Hsieh, and F. Lin, Spatially sparse source cluster modeling by compressive neuromagnetic tomography, Neuroimage, 53 (1), 2010, pp. 146-160.

C. T. Chou, R. Rana, and W. Hu W, Energy efficient information collection in wireless sensor networks using adaptive compressive sensing, IEEE 34th Conference on Local Computer Networks, 2009, pp. 443-450.

I. Daubechies, R. DeVore, M. Fornasier, and S. Gunturk, Iteratively re-weighted least squares minimization: proof of faster than linear rate for sparse recovery, 42nd Ann. Conf. on Inf. Sci. Syst., 2008, pp. 26–29.

R. S. Desikan, F. Ségonne, B. Fischl, B. T. Quinn, B. C. Dickerson, D. Blacker, and R. L. Buckner, An automated labeling system for subdividing the human cerebral cortex on MRI scans into gyral based regions of interest Neuroimage, 31 (3), 2006, pp. 968-980.

L. Ding, Reconstructing cortical current density by exploring sparseness in the transform domain, Physics in medicine and biology, 54 (9), 2009, pp. 2683.

L. Ding, and H. Yuan, Simultaneous EEG and MEG source reconstruction in sparse electromagnetic source imaging, Human brain mapping, 34 (4), 2013, pp. 775-795.

D. L. Donoho, Compressed sensing, IEEE Transactions on Information Theory, 52 (4), 2006, pp. 1289-1306.

B. Efron, T. Hastie, I. Johnstone, and R. Tibshirani, Least angle regression, The Annals of statistics, 32 (2), 2004, pp. 407-499.

Y. C. Eldar, and M. Mishali, Robust recovery of signals from a structured union of subspaces, IEEE Trans. on Information Theory, 55 (11), 2009, pp. 5302–5316.

Y. Eldar, P. Kuppinger, and H. Bolcskei, Block-sparse signals: uncertainty relations and efficient recovery, IEEE Trans. Signal Processing, 58(6), 2010, pp. 3042–3054.

S. Finnigan, and M. J. Putten, EEG in ischaemic stroke: quantitative EEG can uniquely inform (sub-)acute prognoses and clinical management, ClinNeurophysiol1, 24 (1), 2013, pp. 10-19.

J. Friedman, T. Hastie, H. Hofling, and R. Tibshirani, Pathwise coordinate optimization Ann. Appl. Stat. 1, 2004, pp. 302-32.

Friston, K., Harrison, L., Daunizeau, J., Kiebel, S., Phillips, C., Trujillo-Barreto, N., Henson, R., Flandin, G. and Mattout, J., 2008. Multiple sparse priors for the M/EEG inverse problem. NeuroImage, 39(3), pp.1104-1120.

M. Fuchs, J. Kastner, M. Wagner, S. Hawes, and J. S. Ebersole, A standardized boundary element method volume conductor model, Clinical Neurophysiology, 113(5), 2002, pp. 702-712.

N. G. Gençer, and S. J. Williamson, Differential characterization of neural sources with the bimodal truncated SVD pseudo-inverse for EEG and MEG measurements, IEEE Transactions on Biomedical Engineering, 45(7), 1998, pp. 827-838.

T. Goldstein, C. Studer, and R. Baraniuk, A field guide to forward-backward splitting with a FASTA implementation, arXiv preprint arXiv:1411.3406, 2014.

I. F. Gorodnitsky, J. S. George, and B. D. Rao, Neuromagnetic source imaging with FOCUSS: a recursive weighted minimum norm algorithm, Electroencephalography and clinical Neurophysiology, 95 (4), 1995, pp. 231-251.

A. Gramfort, M. Kowalski, and M. Hämäläinen, Mixed-norm estimates for the M/EEG inverse problem using accelerated gradient methods, Physics in medicine and biology, 57 (7), 2012.

R. Grech, T. Cassar, J. Muscat, K. Camilleri, S. Fabri, M. Zervakis, P. Xanthopoulos, V. Sakkalis, and B. Vanrumste, Review on solving the inverse problem in EEG source analysis, Journal of neuroengineering and rehabilitation, 5 (1), 2008.

M. A. Jatoi, N. Kamel, A. S. Malik, I. Faye, and T. Begum, A survey of methods used for source localization using EEG signals. Biomedical Signal Processing and Control, 11, 2014, pp.42-52.

M. A. Jatoi, N. Kamel, A. S. Malik, I. Faye, and T. Begum, Representing EEG source localization using finite element method. IEEE International Conference on in Control System, Computing and Engineering (ICCSCE), 2013, pp. 168-172.

M. A. Jatoi, N. Kamel, I. Faye, A. S. Malik, J. M. Bornot, and T. Begum, BEM based solution of forward problem for brain source estimation. In 2015 IEEE International Conference on Signal and Image Processing Applications (ICSIPA), 2015, pp. 180-185.

M. A. Jatoi, N. Kamel, A. S. Malik, I. Faye, J. M. Bornot, and T. Begum, EEG-based brain source localization using visual stimuli. International Journal of Imaging Systems and Technology, 26 (1), 2016, pp. 55-64.

P. W. Kaplan, and A. O. Rossetti, EEG Patterns and Imaging Correlations in Encephalopathy: Encephalopathy Part II, Journal of Clinical Neurophysiology, 28 (3), 2011, pp. 233-251.

Y. Li, A globally convergent method for l_p problems, SIAM Journal on Optimization, 3(3), 1993, pp. 609–629.

H. Liu, P. H. Schimpf, G. Dong, X. Gao, F. Yang, and S. Gao, Standardized shrinking LORETA-FOCUSS (SSLOFO): a new algorithm for spatio-temporal EEG source reconstruction, IEEE Transactions on Biomedical Engineering, 52 (10), 2005, pp.1681-1691.

J. D. Lopez, G. R. Barnes, and J. J. Espinosa, Single MEG/EEG source reconstruction with multiple sparse priors and variable patches. Dyna, 79(174), 2012, pp.136-144.

J. D. Lopez, V. Litvak, J. J. Espinosa, K. Friston, and G. R. Barnes, Algorithmic procedures for Bayesian MEG/EEG source reconstruction in SPM. NeuroImage, 84, 2014, pp.476-487.

MRIcroAAL http://www.mccauslandcenter.sc.edu/mricro/mricro/template.html

P. L. Nunez, R. B. Silberstein, P. J. Cadusch, R. S. Wijesinghe, A. F. Westdorp, and R. Srinivasan, A theoretical and experimental study of high resolution EEG based on surface Laplacians and cortical imaging, Electroencephalography and clinical neurophysiology, 90 (1), 1994, pp. 40-57.

P. L. Nunez, and R. Srinivasan, Electric fields of the brain: the neurophysics of EEG, Oxford University Press USA, 2006.

M. R. Osborne, B. Presnell, and B. A. Turlach, A new approach to variable selection in least squares problems, IMA journal of numerical analysis, 20(3), 2000, pp. 389-403.

Pascual-Marqui, and R. Domingo, Review of methods for solving the EEG inverse problem, International journal of bioelectromagnetism, 1(1), 1999, pp. 75-86.

T. G. Phan, T. Gureyev, Y. Nesterets, H. Ma and D. Thyagarajan, Novel Application of EEG Source Localization in the Assessment of the Penumbra, Cerebrovascular diseases, 33 (4), 2012, pp. 405-407.

J. W. Phillips, R. M. Leahy, and J. C. Mosher, MEG-based imaging of focal neuronal current sources, IEEE Trans. Med. Imag. 16 (3), 1997, pp. 338-348.

R. D. Pascual-Marqui, Review of methods for solving the EEG inverse problem, International journal of bioelectromagnetism, 1(1), 1999, pp. 75-86.

R. D. Pascual-Marqui, Standardized low-resolution brain electromagnetic tomography (sLORETA): technical details, Methods Find Exp Clin Pharmacol, 24(Suppl D), 2002, pp.5-12.

C. Plummer, A. S. Harvey, and M. Cook, EEG source localization in focal epilepsy: Where are we now? Epilepsia, 49 (2), 2008, pp. 201-218.

S. Saha, Y. Nesterets, M. Tahtali, and T. E. Gureyev, Evaluation of Spatial Resolution and Noise Sensitivity of sLORETA Method for EEG Source Localization Using Low-Density Headsets, Biomedical Physics & Engineering Express 1 (4), 2015.

S. Saha, and M. Tahtali, Compressed Sensing and Its Application in CT and EEG, Biomedical Image Analysis and Mining Techniques for Improved Health Outcomes, 123, 2015b.

S. Saha, Y. I. Nesterets, R. Rana, M. Tahtali, F. de Hoog, and T. E. Gureyev, EEG source localization using a sparsity prior based on Brodmann areas, arXiv:1406.2434, 2014.

S. Saha, F. de Hoog, Y. I. Nesterets, R. Rana, M. Tahtali, and T. E. Gureyev, Sparse Bayesian Learning for EEG Source Localization, arXiv preprint arXiv:1501.04621, 2015c.

J. X. Tao, A. Ray, S. Hawes-Ebersole, and J. S. Ebersole, Intracranial EEG substrates of scalp EEG interictal spikes, Epilepsia, 46 (5), 2005, pp. 669-676.

R. Tibshirani, Regression shrinkage and selection via the lasso, Journal of the Royal Statistical Society Series B (Methodological), 1996, pp. 267-288.

M. E. Tipping, Sparse Bayesian learning and the relevance vector machine, The journal of machine learning research, 1, 2001, pp. 211-244.

N. Tzourio-Mazoyer, B. Landeau, D. Papathanassiou, F. Crivello, O. Etard, N. Delcroix, B. Mazoyer, and M. Joliot, Automated Anatomical Labeling of activations in SPM using a Macroscopic Anatomical Parcellation of the MNI MRI single-subject brain, NeuroImage, 15 (1), 2002, pp. 273-289.

M. Wagner, M. Fuchs, and J. Kastner, Evaluation of sLORETA in the presence of noise and multiple sources, Brain Topography, 16 (4), 2004, pp. 277-280.

B. Wei, M. Yang, R. K. Rana, C. T. Chou, and W. Hu, Distributed sparse approximation for frog sound classification, Proceedings of the 11th international conference on Information Processing in Sensor Networks, 2012, pp. 105-106.

B. Wei, M. Yang, Y. Shen, R. Rana, C. T. Chou, and W. Hu, Real-time classification via sparse representation in acoustic sensor networks, Proceedings of the 11th ACM Conference on Embedded Networked Sensor Systems, 2013.

S. C. Wu, and A. L. Swindlehurst, Matching Pursuit and Source Deflation for Sparse EEG/MEG Dipole Moment Estimation, IEEE Transactions on Biomedical Engineering, 60 (8), 2013, pp. 2280 – 2288.

J. Yao, and J. Dewald, Evaluation of different cortical source localization methods using simulated and experimental EEG data, Neuroimage, 25 (2), 2005, pp. 369-382.

M. Yuan, and Y. Lin, Model selection and estimation in regression with grouped variables, Journal of the Royal Statistical Society: Series B (Statistical Methodology), 68 (1), 2006, pp. 49-67.

Z. Zhang, Comparison of Sparse Signal Recovery Algorithms with Highly Coherent Dictionary Matrices: The Advantage of T-MSBL, Research Note, 2012.

Z. Zhang, and B. Rao, Extension of SBL algorithms for the recovery of block sparse signals with intra-block correlation, IEEE Transactions on Signal Processing, 61 (8), 2013, pp. 2009-2015.

Z. Zhang, and B. D. Rao, Sparse signal recovery with temporally correlated source vectors using sparse Bayesian learning, IEEE Journal of Selected Topics in Signal Processing, 5(5), 2011, pp. 912-926.

Z. Zhang, and B. D. Rao, Recovery of block sparse signals using the framework of block sparse Bayesian learning, 2012 IEEE International Conference on Acoustics, Speech and Signal Processing (ICASSP), 2012, pp. 3345-3348.

K. Zilles, and K. Amunts, Centenary of Brodmann's map—conception and fate, Nature Reviews Neuroscience, 11 (2), 2010, pp. 139-145.

List of captions

Figures

Fig. 1: Positions of the 230 dipoles.

Fig. 2: Number of dipoles per block - (a) Brodmann area based clustering, (b) AAL based clustering.

Fig. 3: Schematic representation of the electrodes positions in the 71-electrodes setup.

Fig. 4: Success rate and localization errors (for unsuccessful cases) of BSBL and SBL methods with respect to different noise levels.

Fig. 5: Success rate and localization error (for unsuccessful cases) of BSBL and SBL methods for simultaneously active multiple blocks.

Fig. 6: Representative reconstructions by BSBL and SBL methods for AAL based blocks for (a) two, (b) three and (c) four simultaneously active blocks.

Fig. 7: Representative reconstructions by BSBL and SBL methods for Brodmann area based blocks for (a) two, (b) three and (c) four simultaneously active blocks.

Fig. 8: Success rate and localization error (for unsuccessful cases) of BSBL method for simultaneously active multiple blocks in the presence of 20 dB noise.

Fig. 9: Mean square error between the actual and reconstructed signal. Left - AAL based blocks, right – Brodmann area based blocks.

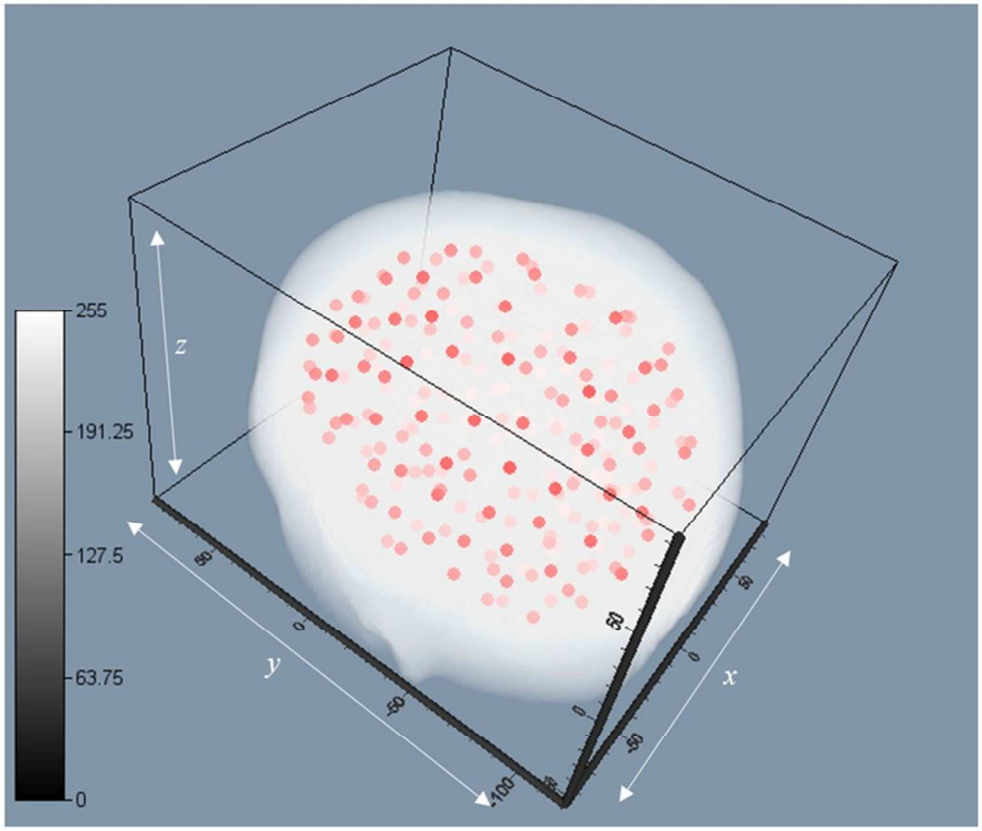

Fig. 1: Positions of the 230 dipoles.

66x56mm (300 x 300 DPI)

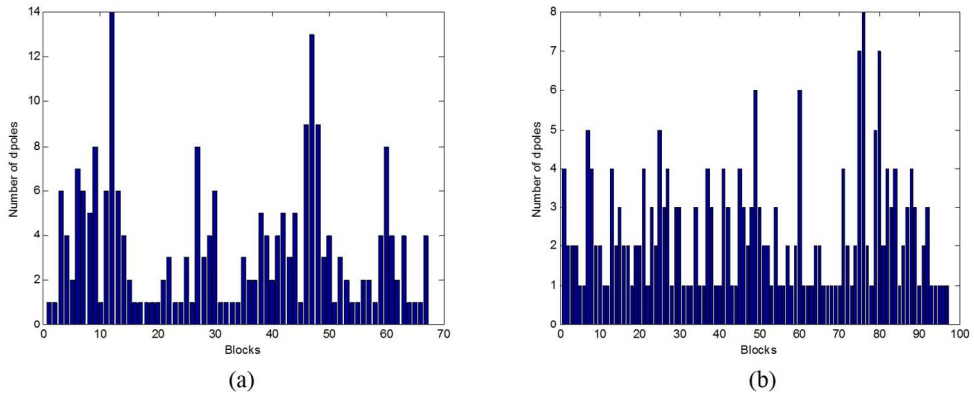

Fig. 2: Number of dipoles per block - (a) Brodmann area based clustering, (b) AAL based clustering.

150x65mm (300 x 300 DPI)

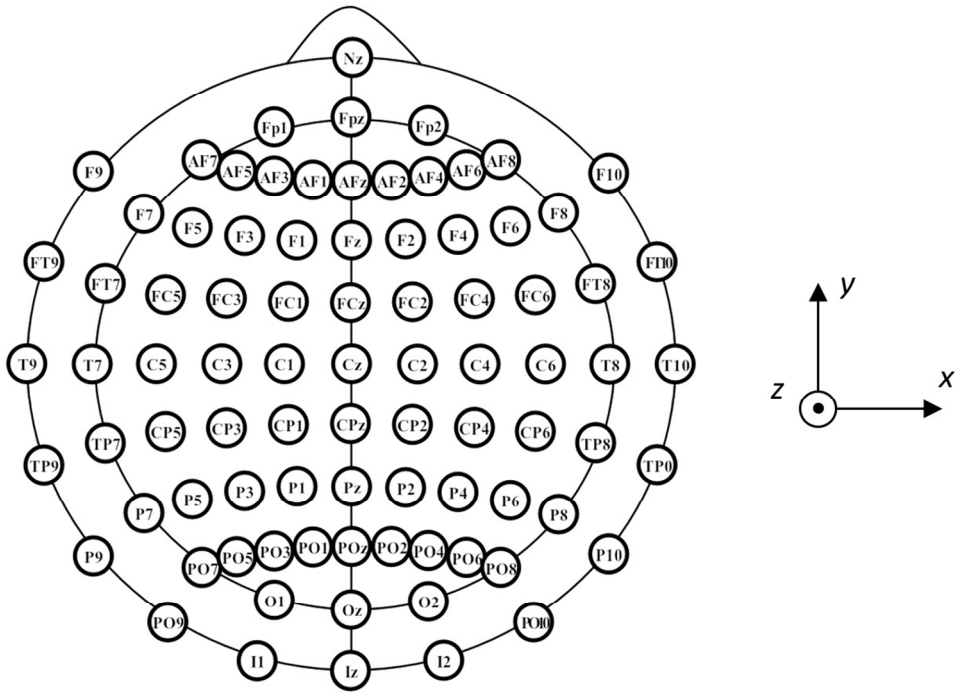

Fig. 3: Schematic representation of the electrodes positions in the 71-electrodes setup.

108x76mm (300 x 300 DPI)

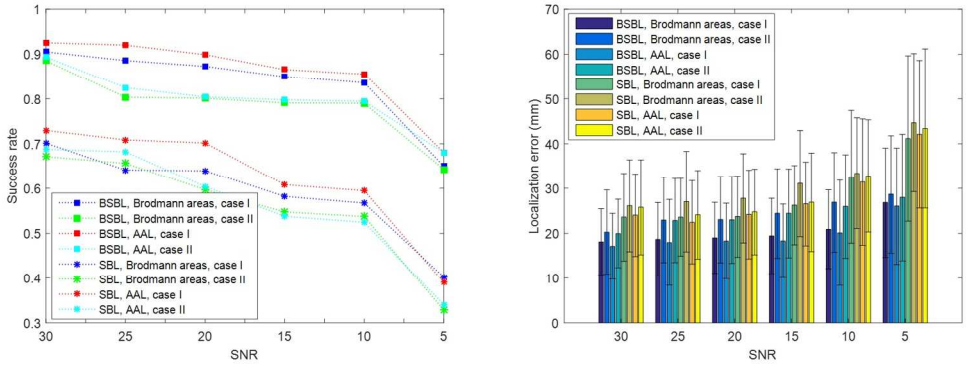

Fig. 4: Success rate and localization errors (for unsuccessful cases) of BSBL and SBL methods with respect to different noise levels.

153x60mm (300 x 300 DPI)

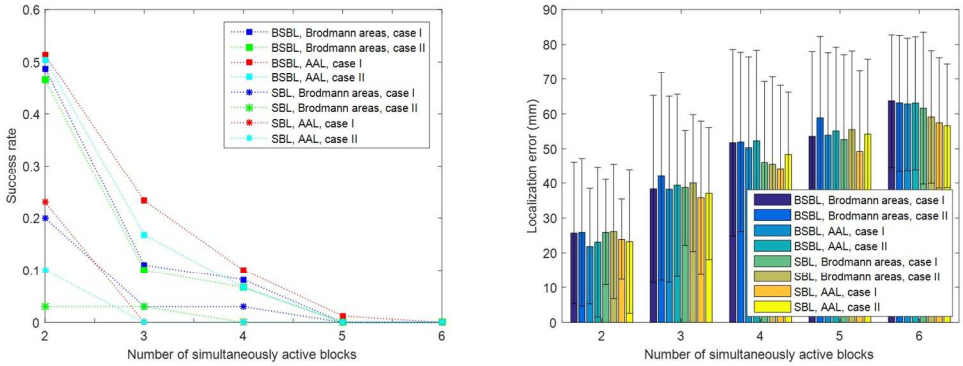

Fig. 5: Success rate and localization error (for unsuccessful cases) of BSBL and SBL methods for simultaneously active multiple blocks.

154x61mm (300 x 300 DPI)

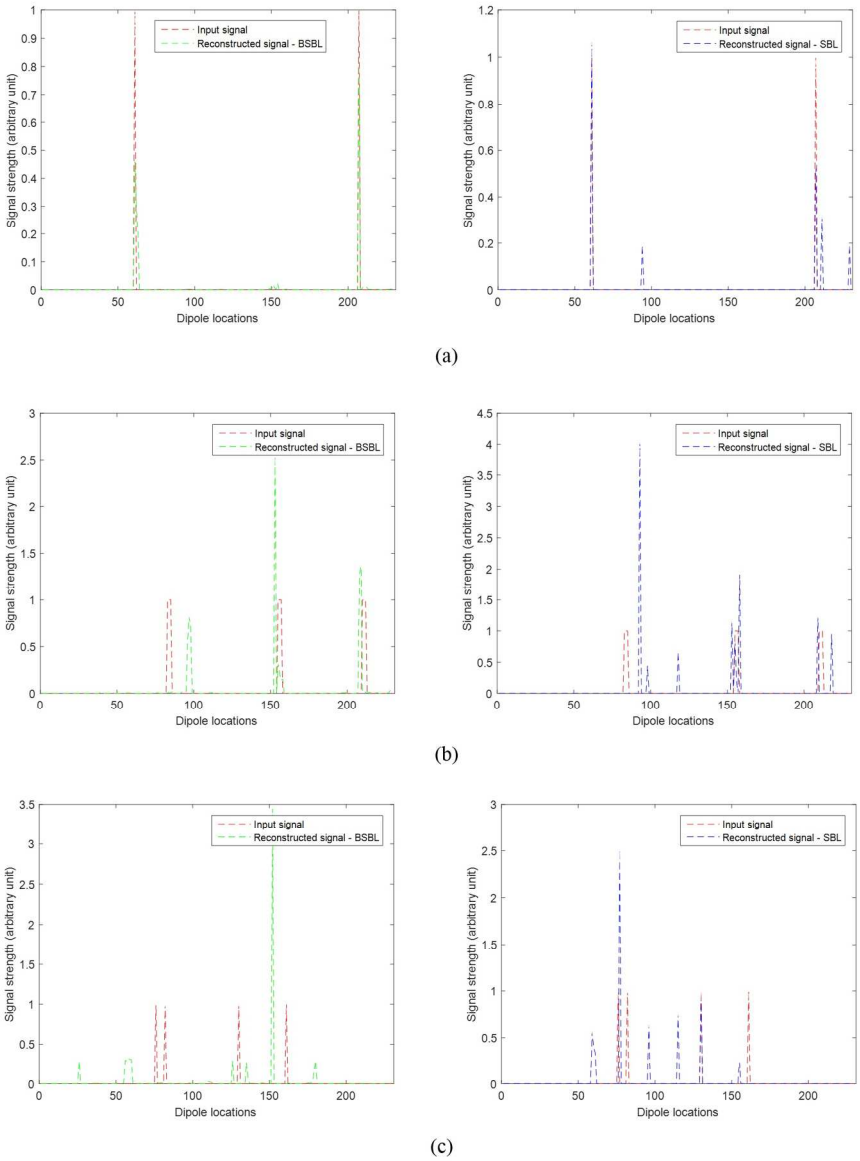

Fig. 6: Representative reconstructions by BSBL and SBL methods for AAL based blocks for (a) two, (b) three and (c) four simultaneously active blocks.

151x206mm (300 x 300 DPI)

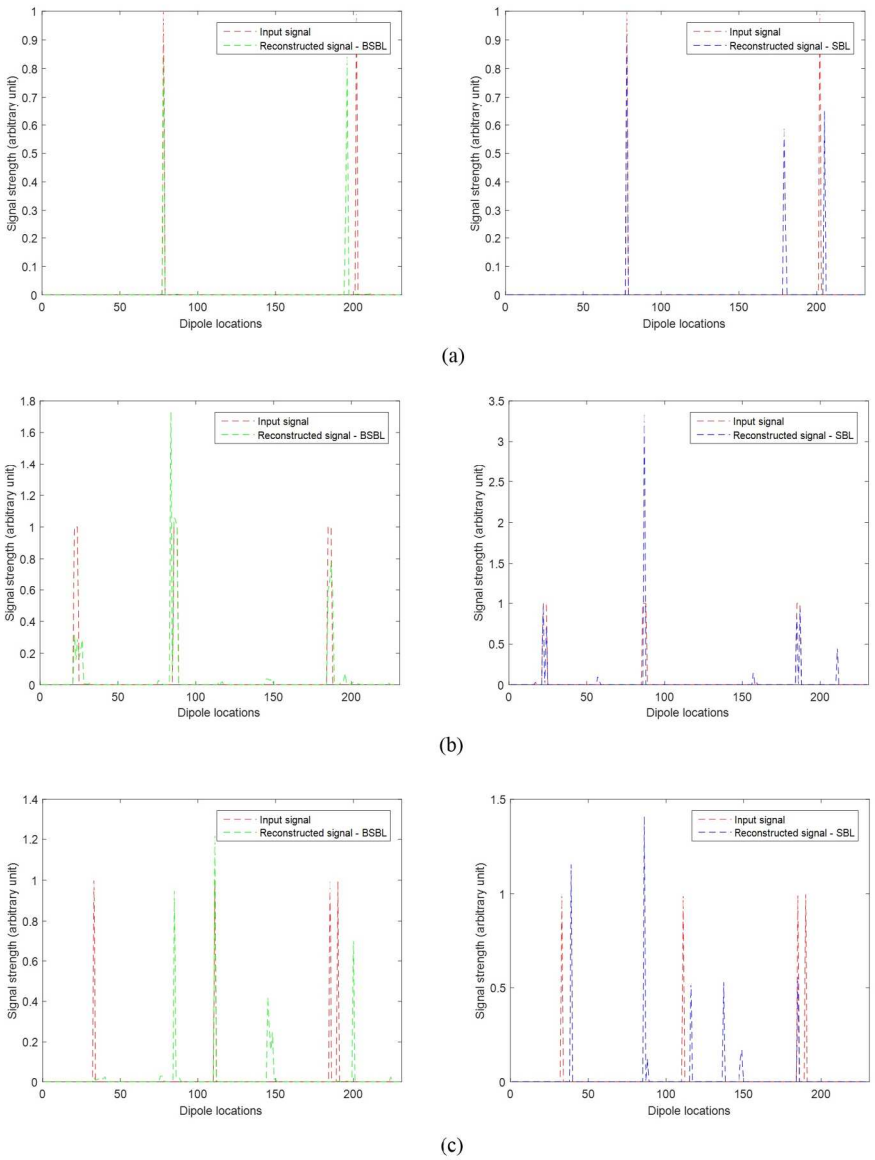

Fig. 7: Representative reconstructions by BSBL and SBL methods for Brodmann area based blocks for (a) two, (b) three and (c) four simultaneously active blocks.

151x203mm (300 x 300 DPI)

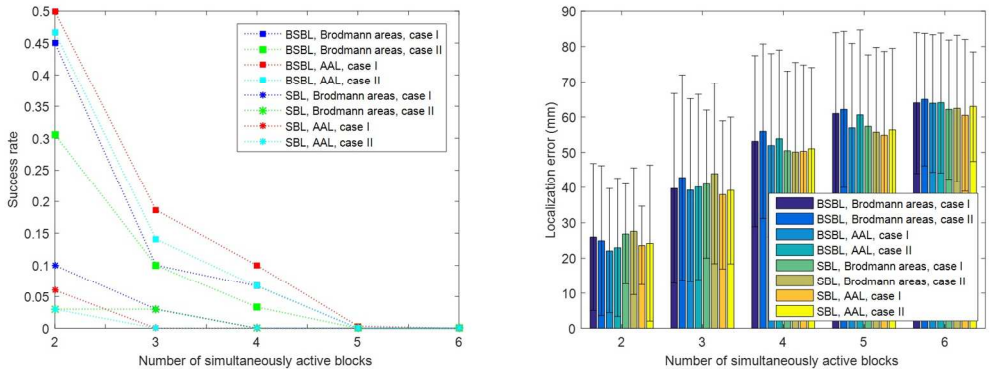

Fig. 8: Success rate and localization error (for unsuccessful cases) of BSBL method for simultaneously active multiple blocks in the presence of 20 dB noise.

151x59mm (300 x 300 DPI)

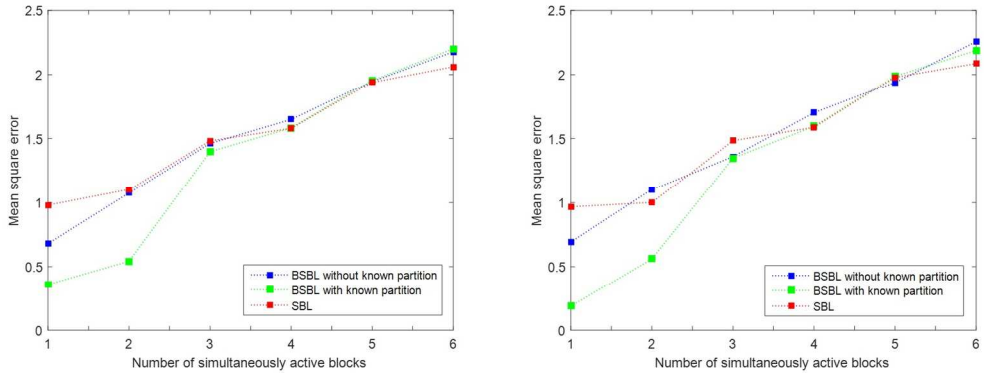

Fig. 9: Mean square error between the actual and reconstructed signal. Left - AAL based blocks, right – Brodmann area based blocks.

150x59mm (300 x 300 DPI)

Table 1: Success rate and localization error of BSBL and SBL methods for a single active block.

Methodology	**Success rate**	**Localization error (mm)**	
		Mean error distance	**Standard deviation**
BSBL, Brodmann area, Case I	0.9394	16.62	7.06
SBL, Brodmann area, Case I	0.7164	22.14	10.35
BSBL, Brodmann area, Case II	0.8507	23.16	10.70
SBL, Brodmann area, Case I	0.6716	23.75	9.78
BSBL, AAL, Case I	0.9507	14.89	5.99
SBL, AAL, Case I	0.7101	21.22	9.09
BSBL, AAL, Case II	0.8547	22.16	10.56
SBL, AAL, Case II	0.6892	26.71	11.23